A Two-Stage Frequency-Voltage Coordinated Emergency Control Strategy for Isolated Microgrids

Yufei Zhao
School of Electrical Engineering
Xi'an Jiaotong University
Xi'an, China
2201412025@stu.xjtu.edu.cn

Jingtao Zhao
State Key Laboratory of Technology and Equipment for Defense against Power System Operational Risks
Nari Technology Co., Ltd.
Nanjing, China
zhaojingtao@sgepri.sgcc.com.cn

Hanwen Gu
School of Electrical Engineering
Xi'an Jiaotong University
Xi'an, China
guhanwen0104@xjtu.edu.cn

Zaibin Jiao
School of Electrical Engineering
Xi'an Jiaotong University
Xi'an, China
jiaozaibin@mail.xjtu.edu.cn

Jiawei Yuan
School of Electrical Engineering
Xi'an Jiaotong University
Xi'an, China
yuanjiawei@xjtu.edu.cn

Zongbo Li
School of Electrical Engineering
Xi'an Jiaotong University
Xi'an, China
lizongbo@xjtu.edu.cn

***Abstract*—This paper proposes a two-stage frequency-voltage coordinated emergency control strategy to improve the transient performance of isolated microgrids under contingencies. In the first stage, distributed generators are rapidly coordinated based on the gradient of power imbalance to suppress further frequency degradation. The second stage employs model predictive control to account for the dynamic differences among various devices, enabling fast and accurate frequency restoration while maintaining voltage quality. Simulation results demonstrate that the proposed strategy effectively reduces the maximum frequency deviation and accelerates system recovery, achieving superior performance compared with single-stage control approaches.**

***Index Terms*—Emergency control, frequency control, isolated microgrid, model predictive control, voltage control**

I. INTRODUCTION

Recently, the large-scale integration of distributed energy resources (DERs) has made microgrids a crucial component of the power system. Isolated microgrids, in particular, have broad application prospects owing to their ability to provide autonomous power supply in remote areas, islands, and post-disaster scenarios [1]–[3]. However, when disconnected from the main grid, microgrids lose external inertia and power support, making them highly vulnerable to power imbalances during sudden events such as critical load switching. These imbalances can lead to severe frequency fluctuations and even threaten system stability. The frequency control of isolated microgrids is further challenged by their multi-energy-carrier nature, various devices coordination, and inherently low inertia characteristics [2].

Microgrids generally adopt a hierarchical control strategy consisting of primary, secondary, and tertiary control stages. The primary control typically relies on droop control to allocate power among distributed generators (DGs) [4]. To enhance frequency performance, various advanced strategies have been proposed, including adaptive droop control [5], virtual synchronous generator (VSG) control [6], [7], among others. These approaches have partially mitigated the frequency issues arising from the high penetration of renewable energy sources. However, they predominantly belong to the differential regulation category, which makes precise frequency restoration difficult. In addition, some studies have utilized the voltage-sensitive loads to regulate frequency in isolated microgrids [8], [9]. Although this method can partially improve frequency performance, it often compromises voltage quality.

To achieve precise frequency restoration and coordinated control among various DGs, optimal and model predictive control (MPC) based strategies have been extensively investigated [10]–[14]. In [10], a stagewise method was proposed that employs measurement-driven optimization strategies in the second and third stages to regulate system voltage and frequency rapidly. In [11], a feedback-based gradient optimization method was developed to suppress frequency fluctuations. The approach in [12] achieved frequency regulation by jointly optimizing the droop coefficients and voltage setpoints of DGs. In [13], an optimal reset control strategy based on linear quadratic regulation (LQR) was proposed to enhance the frequency response and reduce frequency deviations in isolated microgrids. An MPC-based controller is presented in [14] to enhance the transient response of networked microgrids. However, most existing studies focus primarily on small-disturbance scenarios, paying limited attention to rapid dynamic responses under contingencies, and often neglect the inherent differences among DGs.

Based on the discussion above, this paper proposes a two-stage emergency control strategy featuring coordinated frequency-voltage optimization. In the first stage, power imbalance is rapidly allocated based on the gradient to suppress

The work was supported by the Smart Grid-National Science and Technology Major Project (2025ZD0806000).

979-8-3315-8138-1

further frequency deterioration. In the second stage, the MPC-based method is employed to jointly regulate the active power outputs and voltage setpoints of DGs, enabling fast and accurate frequency restoration. Through this stagewise control architecture, the proposed strategy effectively limits frequency deviation and mitigates the impact of sudden disturbances during the initial stage. In the restoration stage, it fully exploits the capabilities of various DGs to achieve coordinated restoration and comprehensive optimization of both frequency and voltage.

The rest of the paper is organized as follows: Section II describes the system model. Section III introduces the two-stage control strategy in detail. The effectiveness of the proposed method is validated by simulation in Section IV. Section V gives the conclusion.

II. Model Description

The studied system consists of SGs, battery energy storage systems (BESSs), photovoltaics (PVs), and loads. Both the BESS and PV are connected to the grid via voltage-source converters (VSCs).

A. Synchronous Generator Model

The SG exhibits complex electromechanical dynamics that play a dominant role in system frequency behavior. To capture these dynamics with appropriate accuracy while maintaining model tractability, this study adopts the third-order SG model as described in [14]:

$$\frac{d\delta}{dt} = \omega_s(\omega - 1) \tag{1}$$

$$2H\frac{d\omega}{dt} = T_M - \frac{P_e}{\omega} - D\omega \tag{2}$$

$$T'_{d0}\frac{dE'_q}{dt} = -E'_q - (X_d - X'_d)I_d + E_f \tag{3}$$

where δ denotes the rotor angle; ω is the rotor angle velocity; ω_s is the nominal value of rotor angle velocity; H is the inertia constant; T_M is the mechanical torque; P_e is the electromagnetic power; D is the damping coefficient; T'_{d0} is the d-axis open-circuit transient time constant; E'_q is the transient electromotive force; X_d and X'_d are the d-axis synchronous and transient reactance, respectively; and E_f represents the field voltage.

According to [15], [16], the exciter, turbine, and governor models are established as shown in Figs. 1–3, respectively.

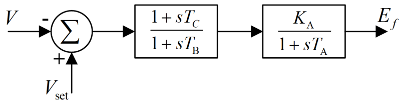

Fig. 1. Exciter model of SG.

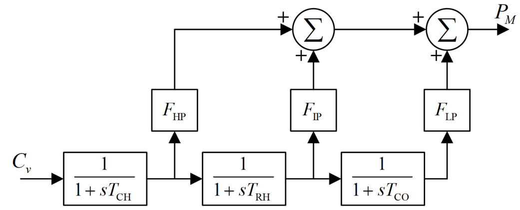

Fig. 2. Turbine model of SG.

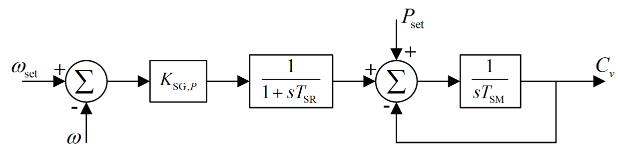

Fig. 3. Governor model of SG.

B. Battery Energy Storage System Model

BESSs are widely used in microgrids and typically participate in primary control through droop control. To simplify the problem, the internal control dynamics of the BESS are neglected in this study, as the BESS's dynamic response is much faster than the microgrid's frequency dynamics, which are dominated by SGs. Accordingly, the BESS is modeled as an ideal controlled power source, whose dynamic behavior can be described by:

$$P_{\text{BESS}} = P_{\text{BESSset}} + K_{\text{BESS},P}(1 - \omega_{\text{BESS}}) \tag{4}$$

$$Q_{\text{BESS}} = Q_{\text{BESS0}} + K_{\text{BESS},Q}(V_{\text{BESSset}} - V_{\text{BESS}}) \tag{5}$$

$$\frac{d\theta_{\text{BESS}}}{dt} = \omega_s(\omega_{\text{BESS}} - 1) \tag{6}$$

where P_{BESS} and Q_{BESS} denote the active and reactive power outputs of the BESS, respectively; P_{BESSset} and Q_{BESS0} represent their corresponding setpoints; ω_{BESS} is the locally measured frequency; V_{BESS} is the terminal voltage; V_{BESSset} is the voltage setpoint; $K_{\text{BESS},P}$ and $K_{\text{BESS},Q}$ are the droop coefficients; and θ_{BESS} is the phase angle obtained from the phase-locked loop (PLL). Since the PLL dynamics are ignored, θ_{BESS} can be regarded as the voltage phase angle at the terminal of the BESS.

C. Photovoltaic Model

As described in [17], PV generally employs maximum power point tracking (MPPT) algorithms to maximize solar energy utilization and typically does not participate in frequency regulation. For simplicity, the PV is assumed to maintain a constant output over a short period and is modeled as a constant power source with unity power factor.

979-8-3315-8138-1

D. Load Model

The load is represented by (7) and (8), which have been commonly adopted in [12] and [14]:

$$P_{\mathrm{L}} = P_{\mathrm{L0}} \left(\frac{V_{\mathrm{L}}}{V_{\mathrm{L0}}} \right)^{n_p} \tag{7}$$

$$Q_{\mathrm{L}} = Q_{\mathrm{L0}} \left(\frac{V_{\mathrm{L}}}{V_{\mathrm{L0}}} \right)^{n_q} \tag{8}$$

where P_{L0}, Q_{L0}, and V_{L0} denote the rated active power, reactive power, and voltage, respectively; while P_{L}, Q_{L}, and V_{L} represent their actual values. The coefficients n_p and n_q depend on the load characteristics. It can be observed that the load power varies with the magnitude of the terminal voltage. Therefore, by adjusting the DG voltage setpoints, the load's active power consumption can be influenced, thereby indirectly affecting the frequency.

E. Power Flow Model

The power injected into bus i is given by:

$$\begin{aligned} P_i &= V_i \sum_{j \in i} V_j \left(G_{ij} \cos\theta_{ij} + B_{ij} \sin\theta_{ij} \right) \\ Q_i &= V_i \sum_{j \in i} V_j \left(G_{ij} \sin\theta_{ij} - B_{ij} \cos\theta_{ij} \right) \end{aligned} \tag{9}$$

where V_i and V_j denote the voltage magnitudes at bus i and j; G_{ij} and B_{ij} represent the conductance and susceptance elements of the admittance matrix, respectively; and $\theta_{ij} = \theta_i - \theta_j$ is the voltage phase angle difference between bus i and j.

By combining the equations above, the state-space model of the isolated microgrid can be established as:

$$\begin{aligned} \dot{\mathbf{x}} &= \mathbf{f}(\mathbf{x}, \mathbf{y}, \mathbf{u}) \\ 0 &= \mathbf{g}(\mathbf{x}, \mathbf{y}, \mathbf{u}) \end{aligned} \tag{10}$$

where $\mathbf{x}$ is the vector of state variables; $\mathbf{y}$ is the vector of algebraic variables; and $\mathbf{u}$ is the vector of control variables. In our study, $\mathbf{u}$ comprises the active power and voltage setpoints of each SG and BESS.

III. Proposed Control Strategy

To address frequency control issues in isolated microgrids under contingencies, this paper proposes a two-stage frequency-voltage coordinated control strategy in which all computations are performed by the microgrid central controller (MGCC). When the frequency deviation exceeds $0.2\,\mathrm{Hz}$ [12], the MGCC immediately activates the first stage control and dispatches control commands to all DGs. Then the MGCC performs the second stage, in which the MPC-based method determines optimal control actions at each sample interval, and the updated commands are subsequently dispatched to all DGs. The proposed method operates continuously until the predefined termination conditions are satisfied. The details of each stage are presented below.

A. Rapid Coordination Stage

To accelerate the generation of control decisions, a simplified model based on the steady-state power balance is formulated in this stage. Specifically, the microgrid is modeled as a single-bus system, where network losses are ignored and voltage magnitudes are assumed to remain uniform throughout the system. The dynamic characteristics of the BESS and SG are omitted, and their outputs are considered to follow their respective reference commands instantaneously [12].

Since frequency deviation fundamentally arises from power imbalance, minimizing the frequency deviation is equivalent to minimizing the total power deviation P_{mis}. Therefore, the gradient $\mathbf{G}$ of P_{mis}^2 with respect to each control variable is calculated to derive the control commands, enabling a rapid reduction of the power imbalance:

$$\begin{aligned} \mathbf{G} = \frac{\partial P_{\text{mis}}^2}{\partial \mathbf{u}_1} = 2P_{\text{mis}} \Bigg(& \sum_{i=1}^{N_{\text{SG}}} \frac{\partial P_{\text{SG},i}}{\partial \mathbf{u}_1} + \sum_{i=1}^{N_{\text{BESS}}} \frac{\partial P_{\text{BESS},i}}{\partial \mathbf{u}_1} \\ & + \sum_{i=1}^{N_{\text{PV}}} \frac{\partial P_{\text{PV},i}}{\partial \mathbf{u}_1} - \sum_{i=1}^{N_{\text{L}}} \frac{\partial P_{\text{L},i}}{\partial \mathbf{u}_1} \Bigg) \end{aligned} \tag{11}$$

where N_{SG}, N_{BESS}, N_{PV} and N_{L} denote the numbers of SGs, BESSs, PVs, and loads, respectively; P_{SG}, P_{BESS}, and P_{PV} represent the active power outputs of the SG, BESS, and PV, while P_{L} denotes the load power; $\mathbf{u}_1$ denotes the first stage control variable. Under the assumption of uniform system voltage, $\mathbf{u}_1$ is defined as:

$$\mathbf{u}_1 = \left[\mathbf{P}_{\text{SG}}^T, \mathbf{P}_{\text{ES}}^T, V \right]^T \tag{12}$$

where V denotes the voltage magnitude shared by all buses.

By combining (7), $\mathbf{G}$ can be obtained as shown in (13).

$$\mathbf{G} = 2P_{\text{mis}} \left[1, \cdots, 1, 2\frac{V}{V_0^2} \sum_{i=1}^{N_{\text{L}}} P_{\text{L0},i} \right]^T \tag{13}$$

To account for the different dynamic response capabilities of various DGs, a weighting matrix $\mathbf{R}_1$ is introduced to modify the gradient $\mathbf{G}$. For example, since SGs exhibit relatively slow dynamic responses and are less suitable for fast power support, their associated weights are typically set higher to reduce their initial participation. The modified gradient $\mathbf{G}'$ is expressed as:

$$\mathbf{G}' = \mathbf{R}_1^{-1} \mathbf{G} \tag{14}$$

Finally, based on the $\mathbf{G}'$, the initial power imbalance P_{mis0} is proportionally allocated to each control variable, while ensuring that all allocations satisfy the constraints.

$$\Delta \mathbf{u} = P_{\text{mis0}} \mathbf{G}' \tag{15}$$

B. Optimization Restoration Stage

Considering the nonlinear characteristics of the isolated microgrid model developed in Section II, it is linearized at the operating point $(\mathbf{x}_0, \mathbf{y}_0, \mathbf{u}_0)$ and discretized with the sample period T_s [18], as shown in (16).

$$\begin{aligned} \dot{\mathbf{x}}_{k+1} &= \mathbf{A}\mathbf{x}_k + \mathbf{B}\mathbf{y}_k + \mathbf{C}\mathbf{u}_k + \tilde{\mathbf{f}} \\ \mathbf{0} &= \mathbf{D}\mathbf{x}_k + \mathbf{E}\mathbf{y}_k + \mathbf{F}\mathbf{u}_k + \tilde{\mathbf{g}} \end{aligned} \tag{16}$$

where k denotes the discrete time; $\mathbf{A}$-$\mathbf{F}$ represent system matrices; and $\tilde{\mathbf{f}}, \tilde{\mathbf{g}}$ are constant vectors expressed as:

$$\begin{aligned} \tilde{\mathbf{f}} &= \mathbf{f}(\mathbf{x}_0, \mathbf{y}_0, \mathbf{u}_0) - \mathbf{A}\mathbf{x}_0 - \mathbf{B}\mathbf{y}_0 - \mathbf{C}\mathbf{u}_0 \\ \tilde{\mathbf{g}} &= -\mathbf{D}\mathbf{x}_0 - \mathbf{E}\mathbf{y}_0 - \mathbf{F}\mathbf{u}_0 \end{aligned} \tag{17}$$

To achieve coordinated restoration of frequency and voltage, the second stage aims to minimize both the frequency deviation and control effort. Accordingly, the following quadratic programming problem is formulated:

$$\begin{aligned} \min_{\mathbf{u}_k} \quad & \sum_{k=0}^{N_p-1} \left(\|\boldsymbol{\omega}_{k+1} - \mathbf{1}\|_{\mathbf{Q}}^2 + \|\mathbf{u}_k - \mathbf{u}_{\text{ref}}\|_{\mathbf{R}_1}^2 \right) \\ \text{s.t.} \quad & \text{Equation (16)}, \\ & \mathbf{V}_{\min} \le \mathbf{V}_k \le \mathbf{V}_{\max}, \\ & \mathbf{u}_{\min} \le \mathbf{u}_k \le \mathbf{u}_{\max} \end{aligned} \tag{18}$$

where N_p is the prediction horizon; $\mathbf{Q}$ and $\mathbf{R}_2$ are the weighting matrices; $\boldsymbol{\omega}$ denotes the set of DG frequencies; $\mathbf{u}_{\text{ref}}$ is the control reference from economic dispatch; and $\mathbf{V}$ represents the set of bus voltage magnitudes.

It is worth noting that, since the proposed strategy serves as an emergency control mechanism with a short operating duration, the BESS's state-of-charge (SoC) constraints are ignored. Furthermore, to reduce prediction errors, the system matrices $\mathbf{A}$-$\mathbf{F}$ and vectors $\tilde{\mathbf{f}}, \tilde{\mathbf{g}}$ are updated at each sample interval rather than using a fixed linearized model.

To achieve rapid frequency restoration, the weighting matrix $\mathbf{Q}$ is set much larger than $\mathbf{R}_2$. To maintain high voltage quality after frequency restoration, the weights assigned to voltage setpoints are set higher than those for other control variables. Additionally, to fully exploit the fast frequency regulation capability of BESS and enhance system resilience against disturbances, the power imbalance is predominantly compensated by SGs after frequency restoration. Therefore, the weights associated with the active power output of SGs are set relatively small.

IV. Case Study

This study employs a modified CIGRE benchmark microgrid to verify the effectiveness of the proposed strategy [11], [12]. As illustrated in Fig. 4, the system comprises 15 buses operating at a nominal voltage of 20 kV and a rated frequency of 50 Hz. The microgrid includes: 3 SGs, with SG_1 rated at 5 MVA, SG_2 and SG_3 rated at 2 MVA; 3 BESSs, with $BESS_1$ rated at 1.5 MVA, $BESS_2$ and $BESS_3$ rated at 1 MVA; 2 PVs, with PV_1 rated at 1 MVA and PV_2 rated at 3 MVA. All loads are modeled as constant-impedance loads with parameters $n_p = n_q = 2$.

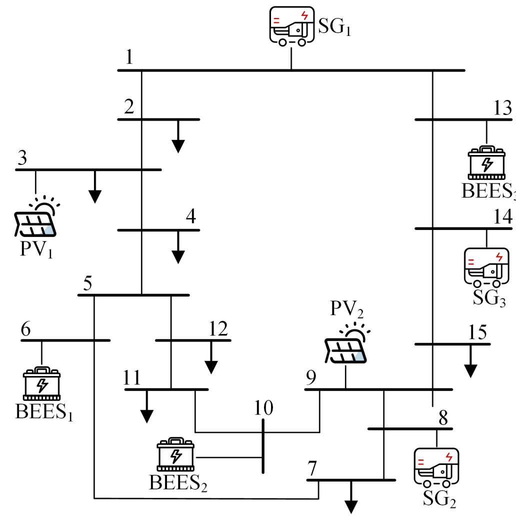

Fig. 4. Modified CIGRE benchmark test microgrid.

We set the sample time to $T_s = 0.5$ s, and the prediction horizon to $N_P = 5$, achieving an appropriate trade-off between control performance and computational efficiency. The dynamics of the microgrids are simulated by PSCAD, while the control algorithm is implemented in MATLAB. All codes are implemented on a PC with a 64-bit Intel Core i7 3.4 GHz CPU and 16 GB of RAM.

In this case, PV_2 is suddenly tripped at 20 s, resulting in a 3 MW power imbalance. As shown in Fig. 5 and Table I, when no corrective action is taken and the system relies solely on primary control, the frequency fails to meet normal operational requirements. The gradient-based allocation strategy effectively mitigates the initial frequency decline but exhibits a relatively slow restoration. In contrast, the MPC-only approach requires longer computation times, causing a lower frequency nadir at the onset of the disturbance and imposing greater stress on the microgrids. The proposed two-stage control strategy achieves both rapid response and high precision, effectively preventing further frequency deterioration while ensuring swift restoration.

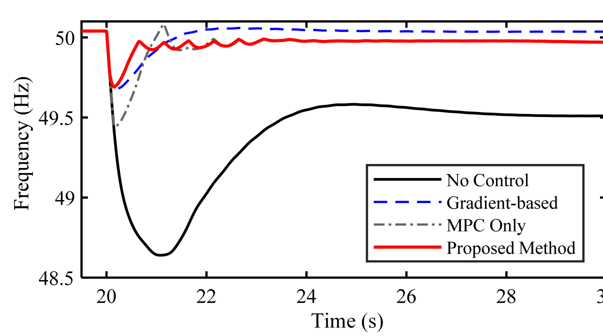

Fig. 5. Microgrid frequency for different strategies during PV_2 trip.

TABLE I
CONTROL PERFORMANCE COMPARISON

Control Strategy	Minimum Frequency (Hz)	Recovery Time to 49.9 Hz (s)
No control	48.64	–
Gradient-based allocation only	49.68	20.9
MPC-only	49.44	20.8
Proposed method	49.69	20.5

As shown in Fig. 6, the proposed strategy allows the BESSs to retain considerable adjustable capacity, enhancing the system's resilience to subsequent disturbances and demonstrating superior resource coordination. Fig. 7 shows the voltage amplitude at bus 15, indicating that the proposed strategy provides improved voltage quality after frequency restoration compared with the gradient-based allocation method. It is also worth noting that the computational time of the first stage is negligible, while the average solution time for each optimization problem in the second stage is approximately $62\,\mathrm{ms}$, satisfying the real-time operational requirements of the proposed control strategy.

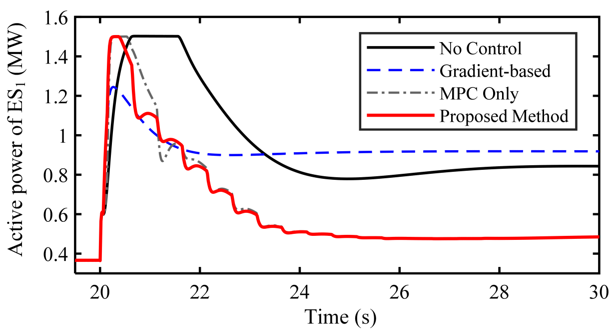

Fig. 6. Output of ES_1 for different strategies during PV_2 trip.

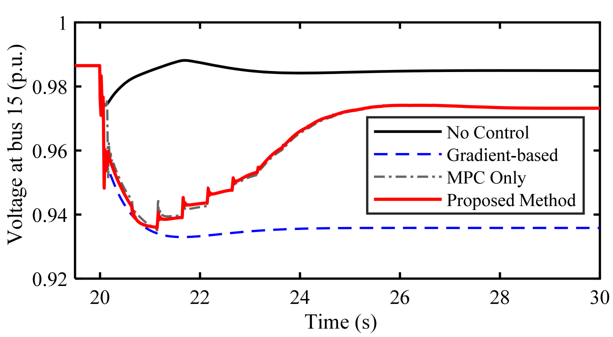

Fig. 7. Voltage at bus 15 for different strategies during PV_2 trip.

V. CONCLUSION

This paper proposes a two-stage frequency-voltage coordinated emergency control strategy to enhance the transient performance of isolated microgrids during contingencies. In the first stage, a gradient-based approach is adopted to rapidly suppress frequency degradation and mitigate the impact of disturbances on the system. In the second stage, an MPC-based method is employed to comprehensively coordinate DGs, enabling fast and accurate frequency restoration while improving voltage quality. Simulation results verify that the proposed control strategy effectively reduces the maximum frequency deviation, achieves coordinated frequency-voltage optimization, and exhibits superior performance compared with single-stage control schemes.

REFERENCES

[1] J. Rocabert, A. Luna, F. Blaabjerg, and P. Rodríguez, "Control of power converters in AC microgrids," *IEEE Transactions on Power Electronics*, vol. 27, no. 11, pp. 4734–4749, 2012.

[2] M. Farrokhabadi *et al.*, "Microgrid stability definitions, analysis, and examples," *IEEE Transactions on Power Systems*, vol. 35, no. 1, pp. 13–29, 2020.

[3] D. E. Olivares *et al.*, "Trends in microgrid control," *IEEE Transactions on Smart Grid*, vol. 5, no. 4, pp. 1905–1919, 2014.

[4] J. M. Guerrero, J. C. Vasquez, J. Matas, L. G. d. Vicuna, and M. Castilla, "Hierarchical control of droop-controlled AC and DC microgrids—a general approach toward standardization," *IEEE Transactions on Industrial Electronics*, vol. 58, no. 1, pp. 158–172, 2011.

[5] S. Prakash, V. Nougain, and S. Mishra, "Adaptive droop-based control for active power sharing in autonomous microgrid for improved transient performance," *IEEE Journal of Emerging and Selected Topics in Power Electronics*, vol. 9, no. 3, pp. 3010–3018, 2021.

[6] M. M. Elwakil, H. M. E. Zoghaby, S. M. Sharaf, and M. A. Mosa, "Adaptive virtual synchronous generator control using optimized bang-bang for islanded microgrid stability improvement," *Protection and Control of Modern Power Systems*, vol. 8, no. 4, pp. 1–21, 2023.

[7] A. Aggarwal, A. Siddiqui, V. Patil, and S. Mishra, "VSG based novel control for interlinking converter in islanded hybrid microgrids," in *2024 23rd National Power Systems Conference (NPSC)*, 2024, pp. 1–6.

[8] B. Alghamdi, "Distributed voltage frequency control of isolated micro-grids," *IEEE Access*, vol. 10, pp. 134 799–134 810, 2022.

[9] M. Farrokhabadi, C. A. Cañizares, and K. Bhattacharya, "Frequency control in isolated/islanded microgrids through voltage regulation," *IEEE Transactions on Smart Grid*, vol. 8, no. 3, pp. 1185–1194, 2017.

[10] Y. Liu, Z. Li, and J. Zhao, "Safety-constrained stagewise optimization of droop control parameters for isolated microgrids," *IEEE Transactions on Smart Grid*, vol. 15, no. 1, pp. 77–88, 2024.

[11] Z. Tang, Y. Liu, T. Liu, G. Qiu, and J. Liu, "Distributed data-driven frequency control in networked microgrids via voltage regulation," *IEEE Transactions on Smart Grid*, vol. 15, no. 5, pp. 4393–4406, 2024.

[12] B. Alghamdi and C. A. Cañizares, "Frequency regulation in isolated microgrids through optimal droop gain and voltage control," *IEEE Transactions on Smart Grid*, vol. 12, no. 2, pp. 988–998, 2021.

[13] Z. Tu, B. Fan, J. Khazaei, W. Zhang, and W. Liu, "Optimal reset-control-based load frequency regulation in isolated microgrids," *IEEE Transactions on Sustainable Energy*, vol. 13, no. 4, pp. 2239–2249, 2022.

[14] K. Liu, T. Liu, Z. Tang, and D. J. Hill, "Distributed MPC-based frequency control in networked microgrids with voltage constraints," *IEEE Transactions on Smart Grid*, vol. 10, no. 6, pp. 6343–6354, 2019.

[15] "IEEE recommended practice for excitation system models for power system stability studies," *IEEE Std 421.5-2016 (Revision of IEEE Std 421.5-2005)*, pp. 1–207, 2016.

[16] I. C. Report, "Dynamic models for steam and hydro turbines in power system studies," *IEEE Transactions on Power Apparatus and Systems*, vol. PAS-92, no. 6, pp. 1904–1915, 1973.

[17] L. Wang *et al.*, "Study on photovoltaic primary frequency control strategy at different time scales," *IET Renewable Power Generation*, vol. 18, no. 16, pp. 3994–4003, 2024. [Online]. Available: https://ietresearch.onlinelibrary.wiley.com/doi/abs/10.1049/rpg2.13100

[18] H. Borhan, A. Vahidi, A. M. Phillips, M. L. Kuang, I. V. Kolmanovsky, and S. D. Cairano, "MPC-based energy management of a power-split hybrid electric vehicle," *IEEE Transactions on Control Systems Technology*, vol. 20, no. 3, pp. 593–603, 2012.